

Compact Octa-band Bandpass Filter based on Controllable Transmission Zeros with Wide Upper Stopband

Qian Yang, Shuangyang Liu, Kai-Da Xu, and Anxue Zhang

School of Information and Communications Engineering
Xi'an Jiaotong University, Xi'an, Shaanxi 710049, China
yangqiandianxin@mail.xjtu.edu.cn, lsy6820@stu.xjtu.edu.cn, kaidaxu@ieee.org, anxuezhang@mail.xjtu.edu.cn

Abstract — A novel synthesis method is proposed to design multi-band bandpass filters (BPFs) using an L-C ladder prototype lowpass filter loaded with two symmetric shorted stubs. The transmission zeros (TZs) are produced by the shorted stubs, which are used to realize multiple passbands. By controlling the number of the open stubs loaded on the shorted stub, the number of TZs is exactly determined. Therefore, multi-band BPF is easy to be obtained by increasing the number of the open stubs. The TZs can be adjusted by optimizing the L-C values of the equivalent circuit of the proposed filter to tune the center frequencies of each passband independently. The proposed BPF also has wide upper stopband. For demonstration, an octa-band BPF is designed and manufactured. The measured results show good agreement with the simulated ones.

Index Terms — Bandpass filters, multi-band, octa-band, transmission zeros, wide upper stopband.

I. INTRODUCTION

With the rapid development of modern communication system, multi-band microwave bandpass filters (BPFs) have gained increasing attentions [1–14]. In order to obtain multiple passbands, multiple single-passband resonators are coupled in parallel with large size [1]. In [2–6], multi-mode resonators (MMRs) have been used to reduce the size. The MMRs use the configuration of stepped-impedance resonator (SIR) or short/open-circuited stubs loaded SIR. Therefore, when the BPF has more passbands, the MMRs have complex structures to excite multiple resonant modes. Another widely used method for designing multi-band BPFs is to synthesize transmission poles (TPs) in passband and transmission zeros (TZs) in stopband or introduce signal-interference to form multiple passbands [7-16]. A tri-notch-band is introduced into a ring-stub multimode resonator to realize multi-band BPF [7]. When the number of the passband grows, more layers of the vertically expendable low-temperature cofired ceramic structure are needed, which increases the fabrication complexity [8]. The tunable TZs in [9-14] can divide one

passband into multiple passbands with center frequency and bandwidth adjusting easily. However, the coupling matrix between the resonators are complicated when the number of passband is increased. The in-series cascade of different reflective-type transversal filtering sections shaped by two in-parallel unequal length transmission line segments are proposed in [15], the structure has a large size when the number of passband increases.

Furthermore, in order to realize wide upper stopband performance, bandstop filters are usually cascaded with BPFs to suppress the spurious response, which are harmful to communication systems [16,17]. Meanwhile, open/shorted coupled lines and transversal signal-interaction concepts are usually adopted to improve the stopband performances [18,19]. However, the sizes are increased and the structures are complicated. Recently, the SIRs in [20,21] with different impedance ratios are presented with compact sizes.

This paper presents a novel synthesis method for designing multiple passbands BPFs by using controllable TZs. Following our early work [22], the theoretical analysis of the TZs and the transmission poles (TPs) is shown in this paper for designing BPF with more passbands. With more degrees of the middle L-C section, more TPs can be positioned in the passbands, which can realized wide passbands. Furthermore, the upper stopband have been also extended with more degrees of middle L-C section. Since the TZs can be independently controlled, the center frequencies (CFs) of each passband can also be independently controlled. However, the bandwidth of each passband cannot be tuned independently. The proposed method for designing multi-band BPF is simple and effective. Due to the filter structure loaded with shorted stubs, the proposed BPF has a wide upper stopband. For demonstration, an octa-band BPF has been designed and fabricated to verify the proposed concept.

II. SYNTHESIS ANALYZE

The proposed multi-band BPF network is shown in Fig. 1. The transmission network can be divided into three sub-networks, which is symmetrical. The middle

section is formed by a lowpass filter (LPF), the equivalent circuit of which is shown in Fig. 2. The middle section consists of five-order LPF. The shunt admittance section is composed of a short-circuited stub loaded with eight open stubs, which is shown in Fig. 3. The equivalent circuit of the shunt stub is shown in Fig. 4, where the loaded open stubs can be equivalent to capacitors and the separated short transmission lines with high characteristic impedance Z_1 can be equivalent to inductors.



Fig. 1. The proposed multi-band BPF network.

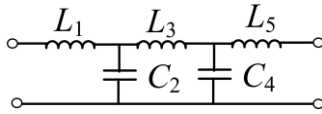


Fig. 2. The equivalent circuit of the middle LPF section.

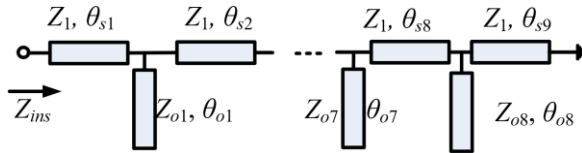


Fig. 3. The shunt admittance section composed by a short-circuited stub loaded with eight open stubs.

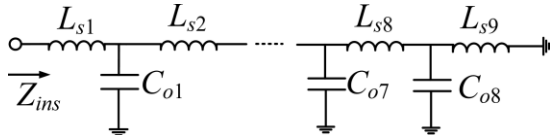


Fig. 4. The equivalent circuit of the parallel stub.

The shunt impedance Z_{ins} can be expressed by the lumped elements in Fig. 4 as follows:

$$Z_{ins}(s) = \frac{a_{17}s^{17} + a_{15}s^{15} + \dots + a_5s^5 + a_3s^3 + a_1s}{b_{16}s^{16} + b_{14}s^{14} + \dots + b_4s^4 + b_2s^2 + b_0}, \quad (1)$$

where a_i and b_i ($i = 0, 1, \dots, 16$) are the constant coefficients, $s = j\omega$ is the radius frequency variable. The coefficients of the numerator and denominator polynomials of equation (1) are all positive real numbers, which can be calculated by the positive L-C values in Fig. 4. The degree of the numerator is 17, which is the number of all the L-C elements. The number can be calculated by the number of the loaded open stubs n , $2n + 1 = 17$, where $n = 8$. Meanwhile, the numerator

polynomial only has odd degree terms.

When the shunt impedance Z_{ins} equals to zero, it introduces short-circuiting effect between the input and output ports, which produces TZs in the frequency response. Therefore, the TZs can be determined by the parameters of the shunt stub. The number of the TZs are the same as that of the numerator degree. Since the numerator polynomial only has odd degree terms, one of the TZs is located at the zero frequency, which is also the direct-current (DC) frequency, and the other sixteen TZs are conjugated and positioned on the frequency axis. As a result, the shunt stub inserts 9 TZs into the LPF positive frequency response and realizes eight passband.

The TPs can be calculated by the approach in [22]. Due to the symmetry of the proposed filter structure, the LPF section parameters are also symmetrical, where $C_4 = C_2$ and $L_5 = L_1$. The TPs can be calculated by the transmission matrix cascaded by the three section in Fig. 1. The degree of the polynomial is the sum of the degree of the two shunt stubs and the degree of the LPF section, which is $2(2n + 1) + 5 = 4n + 7$. From the analysis in [22], the polynomial has one root at origin, two symmetric real roots, and the remaining $4n + 4$ roots are conjugate and symmetrical on the imaginary axis or in four quadrants. Therefore, the BPF has $2n + 2$ TPs at most.

Since the equations for the calculation of TZs and TPs are nonlinear, the optimization algorithm is adapted to calculate the L-C values for design octa-band BPF. Differential evolution algorithm is used in this paper. The optimization goal consists of the positions of TZs and the return losses of each passband, which are set to be larger than 10 dB for easy implementation. After obtaining the L-C values, the electrical length of the open stub θ_{oi} and the electrical length θ_{si} in Fig. 4 are calculated at the center frequency of the first and last passband $f_0 = (f_{01} + f_{08})/2$, where f_{01} and f_{08} are the CFs of the first and eighth passband [23]:

$$\theta_{si} = \arcsin\left(\frac{2\pi f_0 L_{oi}}{Z_1}\right), \quad (2)$$

$$\theta_{oi} = \arctan\left[Z_{oi} 2\pi f_0 C_{oi} - \frac{Z_{oi}}{Z_1} \tan\left(\frac{\theta_{si}}{2}\right) - \frac{Z_{oi}}{Z_1} \tan\left(\frac{\theta_{s,i+1}}{2}\right)\right]. \quad (3)$$

The design guidelines can be described as follows.

1. Due to the specifications of the octa-band, the TZs are determined by the locations of the CFs and the bandwidths, which are positioned nearly at the center of the two adjacent CFs.

2. The values of all L-C elements are optimized by satisfying the return losses (RLs) in each passband.

3. After the equivalent circuit calculation, the physical parameters of the microstrip transmission lines are firstly determined by the equivalent L-C values, and finally optimized by the electromagnetic simulation software HFSS.

III. OCTA-BAND BPF DESIGN

An octa-band BPF is designed to demonstrate the design method. The CFs of the octa-passband are 0.6, 1.6, 2.6, 3.4, 4.0, 4.6, 5.0 and 5.9GHz, respectively. Therefore, the TZs are preset as 0, 0.98, 1.97, 2.81, 3.74, 4.46, 4.99, 5.45, and 7GHz. The optimized L-C values are: $L_{S1} = 0.9981$, $L_{S2} = 3.2471$, $L_{S3} = 2.6099$, $L_{S4} = 3.3404$, $L_{S5} = 2.6263$, $L_{S6} = 2.6421$, $L_{S7} = 2.9019$, $L_{S8} = 2.9040$, $L_{S9} = 3.512$, $L_1 = 2.5879$, $L_3 = 3.8654$ (unit in nH), $C_{O1} = 0.6963$, $C_{O2} = 1.0725$, $C_{O3} = 1.1104$, $C_{O4} = 1.1445$, $C_{O5} = 1.2021$, $C_{O6} = 1.1491$, $C_{O7} = 1.3274$, $C_{O8} = 1.3596$, $C_2 = 0.6755$ (unit in pF). The TZs and TPs are drawn in Fig. 5. The radian frequency variable s is calculated in unit GHz with facility.

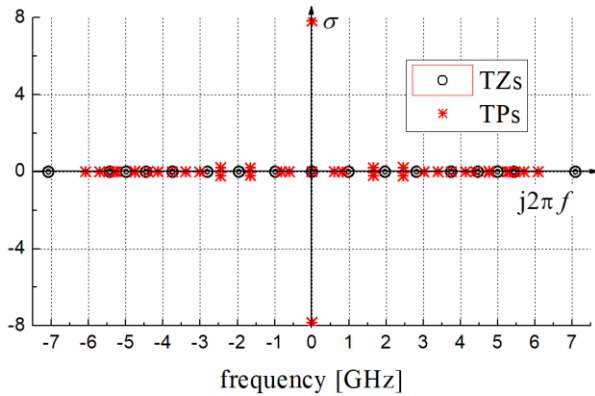


Fig. 5. The calculated TZs and TPs by the equivalent L-C circuit.

All TZs are symmetrical and double values. The $4n+7$ roots related to TPs are conjugate and symmetrical on the axis or in four quadrants, which are consistent with the theoretical analysis in Section II. Three of the roots are real numbers, one of which is at the origin. The remained $4n+4$ roots are distributed symmetrically beside the y axis. Therefore, each passband could have 2 TPs as shown in Fig. 5, and there are still $2((4n+4)/2 - 2n) = 2$, where $n = 8$) roots that can be located freely. One of the remained 2 roots in Fig. 5 is positioned in the eighth passband, while the other one coincides with the fourth TZ.

From Fig. 5, the roots related to TPs in the second and third passbands are two conjugate roots. The related S-parameters calculated by the optimized L-C values are shown in Fig. 6. Therefore, the second and third passbands do not have two TPs as shown in Fig. 6. The eighth passband has three TPs in Fig. 6 as described in Fig. 5. The frequency response in the negative region is not drawn, which is symmetrical to that of the positive region.

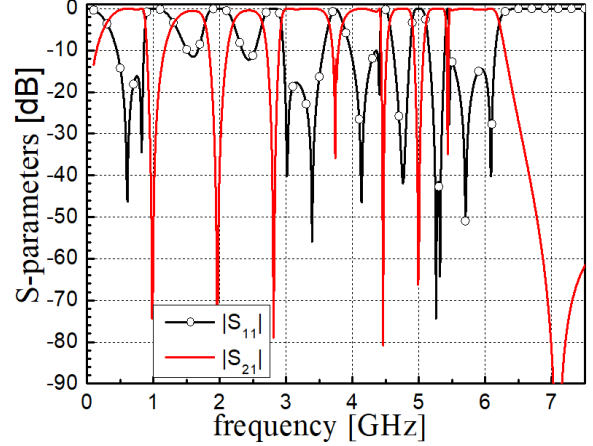


Fig. 6. The calculated S-parameters by optimized L-C values.

IV. EXPERIMENTAL RESULTS

The BPF is simulated and fabricated on a substrate with $\epsilon_r = 2.65$, $\tan\delta = 0.003$, and $h = 1$ mm. Here we choose 117.8Ω high-impedance line and 50Ω low-impedance line, which have the line-width of 0.5 and 2.73 mm, respectively. All the lumped element values are represented by microstrip distributed elements using some equations in [23] at frequency $(f_{01} + f_{08})/2$, where f_{01} and f_{08} are the CFs of the first and eighth passbands, respectively. The configuration of the proposed BPF is shown in Fig. 7. The small part between the two ports is the lowpass filter section as shown in Fig. 1. The two symmetrical shorted stubs are connected to the input and output ports, respectively. The configuration is arranged as a circle to share the same grounded via hole. As shown in Fig. 7, the line width of the open stub which acts as a capacitor is tapered. The characteristic impedance is calculated by the waist width of the taper. Due to the discontinuity of the microstrip line and the minor coupling between the open stubs, the final dimension parameters are optimized by the full-wave electromagnetic simulation software HFSS. The circuit size is about $0.12 \lambda_g \times 0.12 \lambda_g$, where λ_g is the guided wavelength at f_{01} .

Figure 8 shows the simulated and measured S-parameters. The wideband response view and the photograph of the designed filter are shown in Fig. 9 and Fig. 10, respectively. The measured results are in good agreement with the simulated ones. The discrepancies between the simulated results and the measured results may be due to the ignorance of transmission line discontinuity and fabrication tolerances. The measured CFs, fractional bandwidths (FBWs), insertion losses (ILs), and out-band suppressions (OBSs) are listed in Table 1. As shown in Table 1, the proposed octa-band

BPF with simple circuit topology has advantages such as low IL, wide FBW, and wide upper stopband.

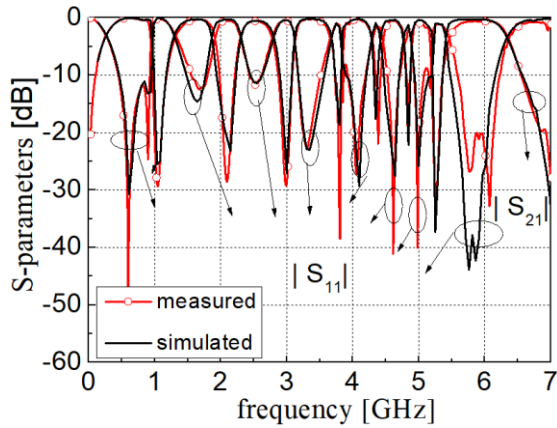


Fig. 8. The passband response view of the designed octa-band BPF.

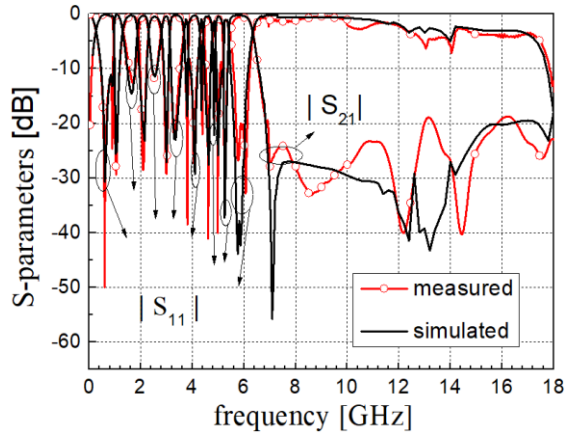


Fig. 9. The wideband response view of the fabricated filter.

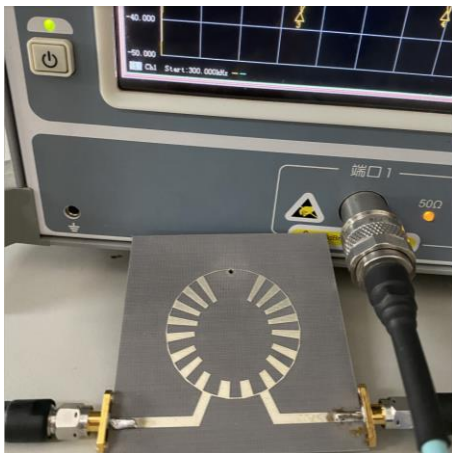


Fig. 10. The fabricated octa-band BPF photograph.

Table 1: Comparisons of proposed filter with related works

Ref.	CF (GHz)/ FBW (%)	IL (dB)	OBS	Size ($\lambda_g \times \lambda_g$)
[1]	0.8/2.3, 1.2/2.9, 1.4/3.3, 1.8/3.2, 2.2/2, 2.5/2	2.9, 2.3, 2.6, 2.2, 2.7, 2.6	--	$0.76 \times$ 0.06
[2]	0.63/29.7, 1.34/8.5, 2.03/2.7, 2.73/5.4, 3.44/6.25, 3.99/9	0.5, 1.3, 1.9, 1.4, 1.2, 1.1	$1.2 f_{06}$, >10dB	0.013 $\times 0.055$
[3]	0.63/28.5, 1.2/10, 1.8/13.6, 2.5/4.8, 3.46/4.2	0.4, 0.9, 1.1, 2, 2.55	$1.1 f_{05}$, >10dB	$0.12 \times$ 0.18
[4]	0.7/10.2, 2/13.2, 3.2/11.3, 4.5/8.1, 5.8/8.2, 7/4.3	1.3, 0.6, 0.8, 1.1, 1.4, 2.2	$1.5 f_{06}$, >15dB	$0.16 \times$ 0.09
This work	0.6/115.2, 1.6/37.5, 2.55/19.6, 3.4/14.4, 4.1/10.3, 4.6/6.7, 5/4.9, 5.9/14.4	0.1, 0.3, 0.6, 0.3, 0.4, 0.6, 0.5, 0.3	$3.1 f_{08}$, >19dB	$0.12 \times$ 0.12

V. CONCLUSION

An octa-band BPF is designed by the method of independently controlling TZs. By optimizing the equivalent circuit lumped elements value, the center frequencies of the octa-passband can be controlled flexibly, making the filter obtain wide passband and wide upper stopband performances. With simple filter structure and good performance, the proposed method is attractive for designing more multi-passband BPFs to apply in modern high data-rate system.

ACKNOWLEDGMENT

This work was supported in part by the National Natural Science Foundation of China under Grant 61801367, and in part by the China Postdoctoral Science Foundation under Grant 2018M631162.

REFERENCES

- [1] W.-H. Tu, and K.-W. Hsu, "Design of sext-band bandpass filter and sext-taplexer using semilumped resonators for system in a package," *IEEE Trans. Compon. Packag. Manuf. Technol.*, vol. 5, no. 2, pp. 265-273, Feb. 2015.
- [2] J. Xu, W. Wu, and G. Wei, "Compact multi-band bandpass filters with mixed electric and magnetic coupling using multiple-mode resonator," *IEEE Trans. Microw. Theory Tech.*, vol. 63, no. 12, pp. 3909-3919, Dec. 2015.
- [3] C. Zhu, J. Xu, W. Kang, and W. Wu, "Compact QB-BPF based on single PMR," *Electron. Lett.*, vol. 52, no. 17, pp. 1463-1465, Aug. 2016.
- [4] J. Ai, Y. Zhang, K.-D. Xu, Y. Guo, and Q.-H. Liu, "Compact sext-band bandpass filter based on single multimode resonator with high band-to-band isolations," *Electron. Lett.*, vol. 52, no. 9, pp. 729-731, Apr. 2016.
- [5] P. Ma, B. Wei, J. Hong, Z. Xu, X. Guo, B. Cao, and L. Jiang, "A design method of multimode multiband bandpass filters," *IEEE Trans. Microw. Theory Tech.*, vol. 66, no. 6, pp. 2791-2799, June 2018.
- [6] T. Firmansyah, M. Alaydrus, Y. Wahyu, E. T. Rahardjo, and G. Wibisono, "A highly independent multiband bandpass filter using a multi-coupled line stub-SIR with folding structure," *IEEE Access*, vol. 8, pp. 83009-83026, May 2020.
- [7] Y. Li, W. Li, C. Liu, and Q. Ye, "A compact UWB band-pass filter with ultra-narrow tri-notch-band characteristic," *Applied Computational Electromagnetics Society (ACES) Journal*, vol. 29, no. 2, pp. 170-177, Feb. 2014.
- [8] Y.-C. Lin, T.-S. Horng, and H.-H. Huang, "Synthesizing a multiband LTCC bandpass filter with specified transmission- and reflection-zero frequencies," *IEEE Trans. Microw. Theory Tech.*, vol. 62, no. 12, pp. 3351-3361, Dec. 2014.
- [9] D. Psychogiou, R. Gómez-García, and D. Peroulis, "Fully adaptive multiband bandstop filtering sections and their application to multifunctional components," *IEEE Trans. Microw. Theory Tech.*, vol. 64, no. 12, pp. 4405-4418, Dec. 2016.
- [10] R. Gómez-García, A. C. Guyette, D. Psychogiou, E. J. Naglich, and D. Peroulis, "Quasi-elliptic multi-band filters with center frequency and bandwidth tunability," *IEEE Microw. Wireless Compon. Lett.*, vol. 26, no. 3, pp. 192-194, Mar. 2016.
- [11] D. Psychogiou, R. Gómez-García, and D. Peroulis, "RF wide-band bandpass filter with dynamic in-band multi-interference suppression capability," *IEEE Trans. Circuits and Systems-II: Express Briefs*, vol. 65, no. 7, pp. 898-902, July 2018.
- [12] R. Gómez-García, J.-M. Muñoz-Ferreras, and D. Peroulis, "High-order input-reflectionless bandpass/ bandstop filters and multiplexers," *IEEE Trans. Microw. Theory Tech.*, vol. 67, no. 9, pp. 3683-3695, Sep. 2019.
- [13] D. J. Simpson, R. Gómez-García, and D. Psychogiou, "Single-/multi-band bandpass filters and duplexers with fully reconfigurable transfer-function characteristics," *IEEE Trans. Microw. Theory Tech.*, vol. 67, no. 5, pp. 1854-1869, May 2019.
- [14] R. Gómez-García, L. Yang, and J.-M. Muñoz-Ferreras, "Low-reflection signal-interference single- and multipassband filters with shunted lossy stubs," *IEEE Microw. Wireless Compon. Lett.*, vol. 30, no. 4, pp. 355-358, Apr. 2020.
- [15] E. Musonda, R. A. Paradkar, I. C. Hunter, and R. Parry, "Synthesis of multiband filters by linear optimization," *IEEE Trans. Microw. Theory Tech.*, vol. 67, no. 12, pp. 4764-4772, Dec. 2019.
- [16] C.-W. Tang and M.-G. Chen, "A microstrip ultra-wideband bandpass filter with cascaded broadband bandpass and bandstop filters," *IEEE Trans. Microw. Theory Tech.*, vol. 55, no. 11, pp. 2412-2418, Nov. 2007.
- [17] H. W. Wu, M. H. Weng, Y. K. Su, C. Y. Hung, and R. Y. Yang, "Spurious suppression of a dual-mode bandpass filter using simple C-shaped electromagnetic bandgap cells," *Microw. Opt. Technol. Lett.*, vol. 48, no. 10, pp. 2090-2093, Oct. 2006.
- [18] W. Feng, M. Hong, and W. Che, "Narrow-band bandpass filters with improved upper stopband using open/shorted coupled lines," *Applied Computational Electromagnetics Society (ACES) Journal*, vol. 31, no. 2, pp. 152-158, Feb. 2016.
- [19] R. Yin, W. Feng, and W. Che, "High selectivity dual-band bandpass filters using dual-mode resonators," *Applied Computational Electromagnetics Society (ACES) Journal*, vol. 32, no. 9, pp. 800-805, Sep. 2017.
- [20] S. Jun and K. Chang, "Second harmonic suppression bandpass filter using nonuniform open stubs," *Microw. Opt. Technol. Lett.*, vol. 55, no. 7, pp. 1451-1453, July 2013.
- [21] J. Marimuthu, A. M. Abbosh, and B. Henin, "Bandpass filter with wide stopband using loaded short-section of parallel-coupled lines," *Microw. Opt. Technol. Lett.*, vol. 57, no. 12, pp. 2824-2829, Dec. 2015.
- [22] Q. Yang, Y.-C. Jiao, and Z. Zhang, "Dual-wideband BPF with wide upper stopband using shorted stepped-impedance stub-loaded lowpass filter," *Electron. Lett.*, vol. 52, no. 19, pp. 1615-1616, Sep. 2016.
- [23] J.-S. Hong and M. J. Lancaster, *Microstrip Filters for RF/Microwave Applications*, Wiley, New York, NY, 2001.